Trends in ^{44}Ti and ^{56}Ni from Core-Collapse Supernovae

Georgios Magkotsios[1,4], Aimee Hungerford[2], Chris Fryer[2], Patrick Young[3] & F. X. Timmes[3,4]

[1]Depart of Physics, University of Notre Dame, Notre Dame, IN 46556; [2]Los Alamos National Laboratories, Los Alamos, NM;
[3]School of Earth and Space Exploration, Arizona State University, Tempe, AZ; [4]Joint Institute for Nuclear Astrophysics

We investigate trends in the yields of ^{44}Ti and ^{56}Ni as material with a specified initial neutron-to-proton ratio cools and rarefies along exponential, power-law, and post-processing thermodynamic trajectories. We use the exponential and power-law expansion profiles to identify 6 distinct regions in the peak temperature-density plane and extensively probe the sensitivity of the isotopic yields to the input nuclear physics. Existence of the 6 regions are largely driven by different phase transitions within the quasi-statistical equilbrium cluster as the material undergoes freeze-out. Most Si-group and Fe-group isotopes are affected by the transitions, with the exception of a small group centralized around ^{56}Ni. Reactions that affect all yields globally are the 3α, p(e^-,nu_e)n and n(e^+,$nubar_e$)p, while ^{44}Ti is mainly affected by ^{44}Ti(α,p)^{47}V, ^{40}Ca(α,Υ)^{44}Ti and ^{45}V(p, Υ)^{46}Cr. Trends due to electron fraction variations may be largely explained in terms of an empirical rule for the major nuclear flows where the most abundant isotopes at any given time in the thermodynamic evolution are generally the ones whose individual proton to nucleon ratio is within a small range from the current value of the electron fraction in combination with a minimization of the Helmholtz free energy. We compare the yields of ^{44}Ti and ^{56}Ni produced from post-processing the thermodynamic trajectories from three different core-collapse models - a Cas A progenitor, a double shock hypernova progenitor, and a rotating 2D explosion - with the yields from the exponential and power-law trajectories. The peak temperatures and densities achieved in these core-collapse models span several of the 6 regions we identify, resulting in different trends in the ^{44}Ti and ^{56}Ni i yields for different mass elements The ^{44}Ti and ^{56}Ni mass fraction profiles from the exponential and power-law profiles generally explain the tendencies of the post-processed yields, depending on which regions are traversed by the model. We find integrated yields of ^{44}Ti and ^{56}Ni from the exponential and power-law trajectories are generally within a factor 2 or less of the post-process yields. Our analysis suggests that not all ^{44}Ti need be produced in an α-rich freeze-out in core-collapse events, and that that reaction rate equilibria in combination with timescale effects for the expansion profile may account for the paucity of ^{44}Ti observed in supernovae remnants.

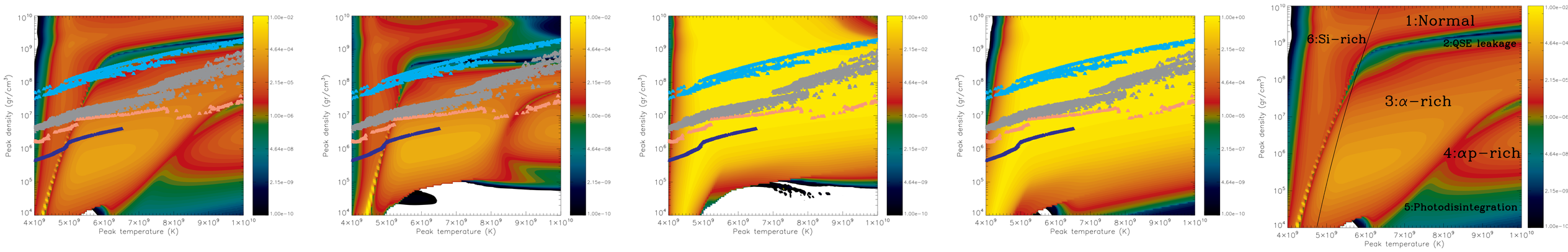

Figure 1: Final ^{44}Ti and ^{56}Ni mass fraction in the peak-temperature-density plane and the 6 physical regions for Y_e=0.5. Overlaid are the peak consition for a 1D Cas A model (blue), a 1D double-shock hypernova model (pink), a 2D rotating 15 $M_\odot$ progenitor (grey), and a 2D MHD collapsar model (cyan).

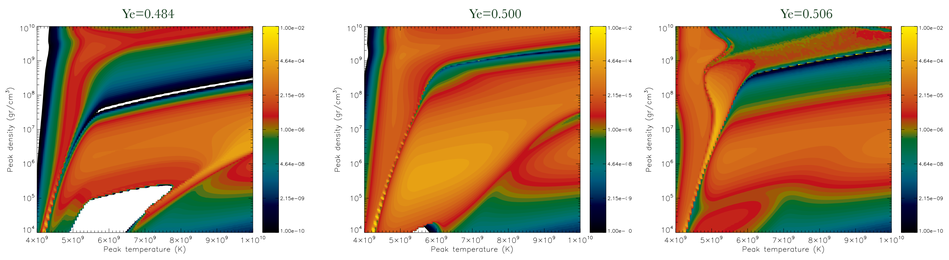

Figure 2: Final yield of ^{44}Ti in the peak temperature-density plane for different initial electron fractions for the exponential freeze-out profile.

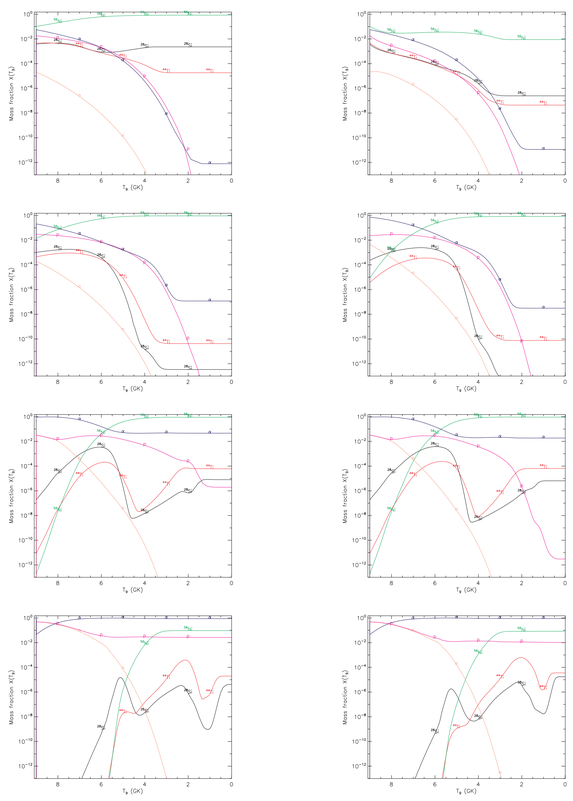

Figure 3: Evolution of ^{28}Si, ^{44}Ti, ^{56}Ni, n, p, and α for the exponential (left) and power-law (right) expansions at Y_e=0.5.

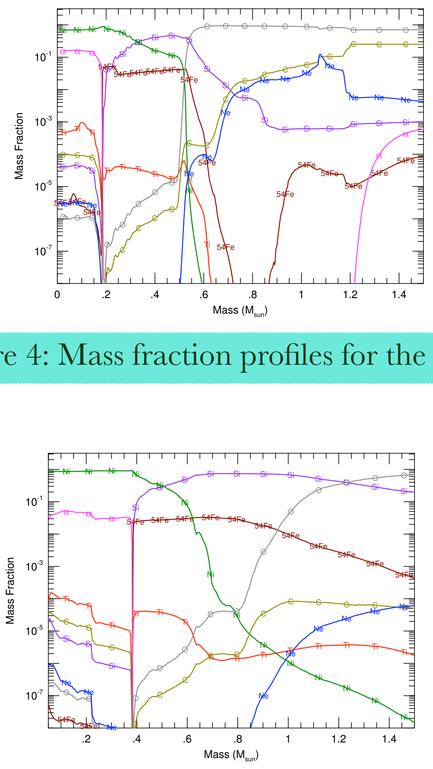

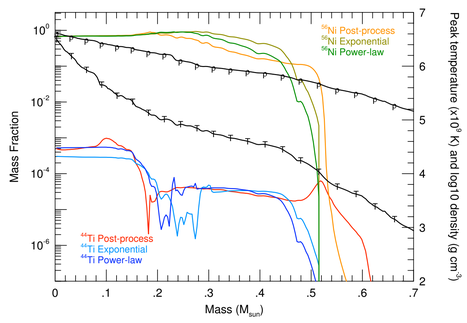

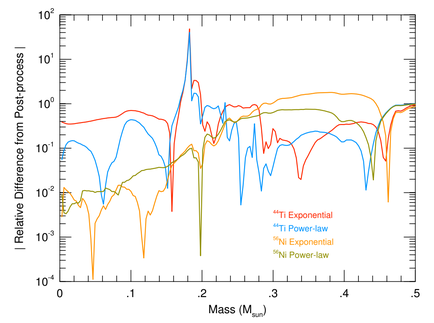

Figure 4: Mass fraction profiles for the exponential, power-law, and post-process trajectories of the Cas A model.

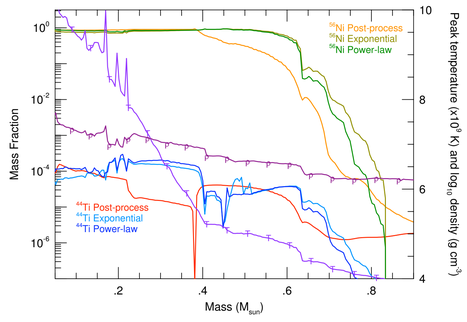

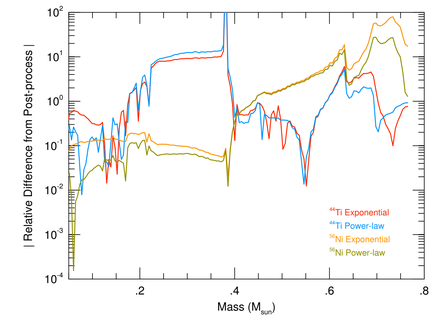

Figure 5: Mass fraction profiles for the exponential, power-law, and post-process trajectories of the hypernova model.

	^{44}Ti Post process ($M_\odot$)	^{44}Ti Exponential ($M_\odot$)	^{44}Ti Power-Law ($M_\odot$)	^{56}Ni Post Process ($M_\odot$)	^{56}Ni Exponential ($M_\odot$)	^{56}Ni Power-Law ($M_\odot$)
Cas A	1.04x10^{-4}	5.62x10^{-5}	9.30x10^{-5}	0.246	0.316	0.278
Hypernova	2.66x10^{-5}	5.23x10^{-5}	6.34x10^{-5}	0.377	0.483	0.497
2D rotating	6.98x10^{-5}	5.09x10^{-5}	4.82x10^{-5}	0.389	0.399	0.410

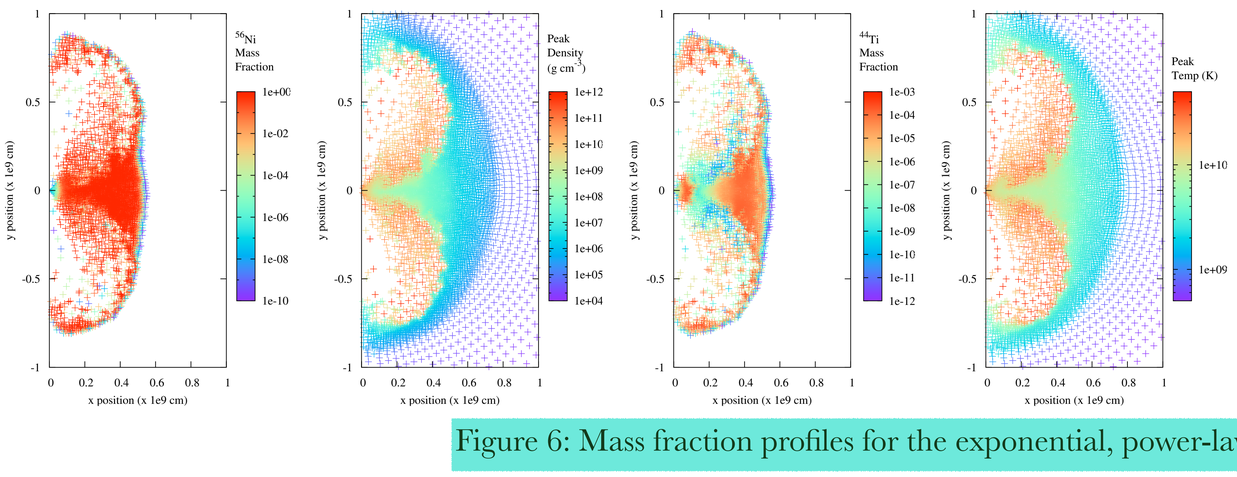

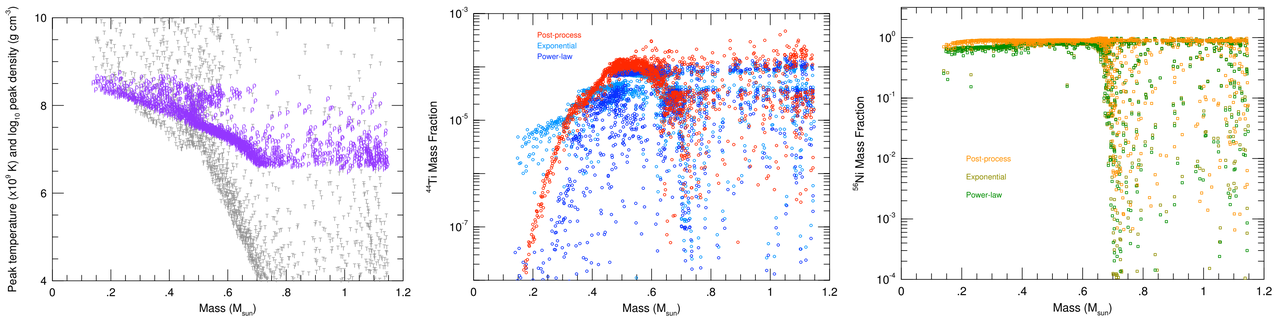

Figure 6: Mass fraction profiles for the exponential, power-law, and post-process trajectories of the rotating 2D 15 $M_\odot$ model.